TuijinJishu/Journal of Propulsion Technology
ISSN: 1001-4055
Vol. 44 No.6 (2023)

Electrochemical and Photocatalytic Properties of Biosynthesized Alkaline Earth Metal Doped Titanium Dioxide Nanoparticles

V. Annapushpam Sangeetha[a*, d], S. Kanagaprabha[b,d], P. N. Selvakumar[c,d]

[a] *Research Scholar, Reg. No. 20212102132010, PG & Research Department of Physics, Pope's College (Autonomous), Sawyerpuram, Thoothukudi-628251, Tamilnadu, India.*

[b] *Associate Professor, Department of Physics, Kamaraj College, Thoothukudi-628003, Tamilnadu, India.*

[c] *Assistant Professor, PG & Research Department of Physics, Pope's College (Autonomous), Sawyerpuram, Thoothukudi-628251, Tamilnadu, India.*

[d] *Affiliated to Manonmaniam Sundaranar University, Abishekapatti, Tirunelveli-627012, Tamilnadu, India.*

Abstract: - Magnesium doped TiO_2 nanoparticles were effectively prepared using green synthesis approach. The synthesised Mg-TiO_2 nanoparticles are examined using XRD, UV-Vis, FTIR, EDX, electrochemical and Photocatalytic activity techniques. The structure, average crystalline size, dislocation density and microstrain were revealed by powder X-ray diffraction. The FTIR analysis indicates the presence of the vibrational modes of the Ti-O-Mg bond. The morphology of the sample was confirmed by SEM. The presence of Ti, O and Mg was analysed by the EDX spectrum. The specific capacitance of the prepared sample was calculated at various scan rates by cyclic voltammetry. The percentage of degradation was analysed by the photocatalytic activity.

Keywords*: Mg doped TiO_2, green synthesis, Solanum torvum, photocatalytic degradation.*

1. Introduction

Nanotechnology is a rapidly growing field that is being used in science and technology to produce new materials at the nanoscale level. Recently, nanoparticles have gained importance and had an impact on the fields of chemical, electronic, energy and biological sciences. These particles can be produced through physical, chemical, or biological processes, although the latter has gained in prominence recently. Because green methods have fewer environmental repercussions than chemical agents, they are more suitable for the preparation of nanoparticles. Plant extracts may act as both capping and reducing agents in the formation of nanoparticles [1-4]. Metal and metal oxide nanoparticles have a high surface-to-volume ratio, which is responsible for their attractive characteristics like antibacterial, magnetic, electrical and catalytic activity. Metal oxides have received a lot of attention due to their unique physicochemical characteristics [5]. Titanium dioxide is an n-type semiconductor with a 3.2 eV broad band gap, excellent chemical and thermal stability and UV light absorption. Titanium dioxide (TiO_2) nanoparticles are one of the most essential materials for photocatalysts [6-7]. Titanium dioxide (TiO_2) is one of the most fascinating metal oxides due to its nontoxic, low-cost and eco-friendly properties, as well as its unique semiconducting and photocatalytic properties. Because of this, it has been effectively employed as a pigment, catalyst in solar cells, sunscreens, pharmaceuticals, and drugs [8]. It oxidizes both organic and inorganic substances in air and water, which causes organic compounds to decompose through redox reactions. TiO_2 has super hydrophilicity, non-toxic, chemically stable and has high energy conversion efficiency when compared to other photocatalysts [9].

In the current study, magnesium doped TiO_2 nanoparticles were prepared by green synthesis method. The synthesised nanoparticles were examined by XRD, UV-Vis, FTIR, SEM, EDX and electrochemical analysis. The photocatalytic activity of magnesium doped TiO_2 nanoparticles was analysed by Methylene Blue (MB) and Congo Red (CR).

2. Green Synthesis of Mg doped TiO_2 nanoparticles

1M of Magnesium Chloride ($MgCl_2$) was dissolved in 50 ml of distilled water and added to the 1M of Titanium Tetrachloride ($TiCl_4$) and 50 ml of Solanum torvum leaf extract. Then it was stirred for two hours at 80ºC using a hot-plate magnetic stirrer. While stirring, 10 mL of NaOH were added dropwise to the mixture to maintain the pH level. White precipitation formed and was filtered out with Whatmann filter paper. The filtered material was washed three times with acetone and double-distilled water and then dried in the open air for two days. Then it was calcinated at 500°C for 5 hours. Figure 1 depicts a graphical representation of the synthesis of Mg doped TiO_2 nanoparticles using Solanum torvum leaf extract.

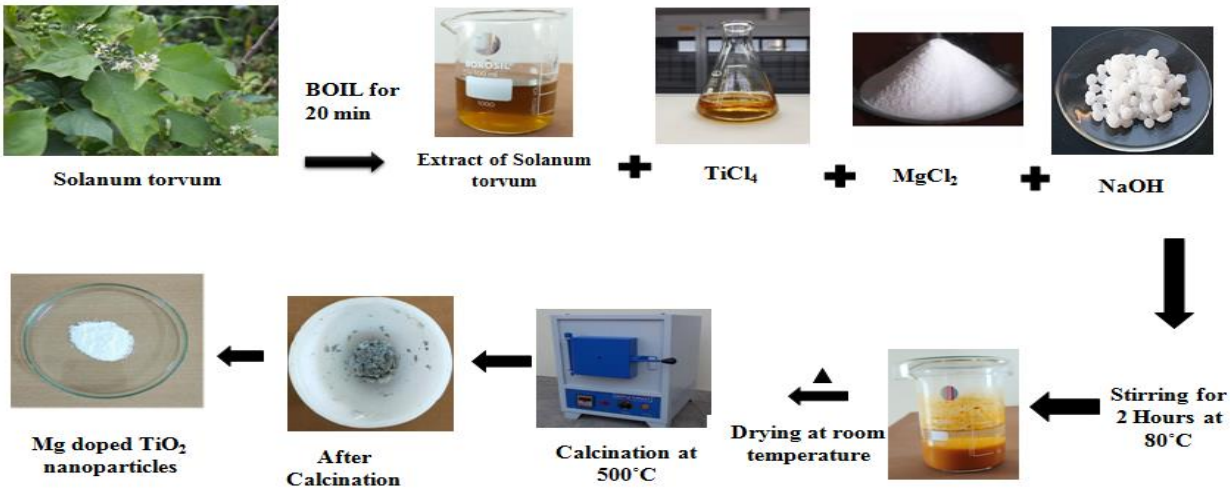

Figure 1. Graphical representation of Mg doped TiO_2 nanoparticles using Solanum torvum leaf extract.

3. Result and Discussion

3.1 Powder X-Ray Diffraction (XRD)

The X-ray Diffractometer was used to analyse the synthesised Mg doped TiO2 nanoparticles. In powder XRD, the CuK_α (λ = 1.5406 Å) radiation source is used and the results were obtained in the range of 10° to 80°. The well defined peaks are found at 25.38, 31.68, 40.57, 45.41, 53.63, 56.31, 62.54 and 75.14 and they are associated with the hkl planes (101), (121), (240), (331), (511), (521), (402) and (721) respectively. The JCPDS card number 35-0792 is well matched with the indexed peaks with (h k l) values. The Scherrer equation was used to estimate the crystalline size [10]. The average crystalline size was found to be 26 nm. The prepared nanomaterial has an orthorhombic structure and its lattice parameters are a = 9.750 Å, b = 9.980 Å, and c = 3.748 Å. The evaluated values of crystallite size, micro strain and dislocation density are listed in table 1 and the XRD pattern of the Mg doped TiO_2 nanoparticles are shown in figure 2.

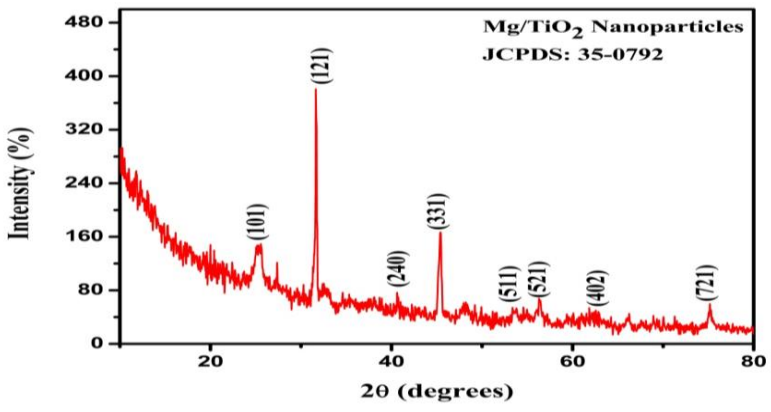

Figure 2. XRD Pattern of Mg doped TiO_2 nanoparticles

The dislocation density values are calculated using the equation [11]

$$\delta = \frac{1}{D} \quad (1)$$

The micro strain is evaluated using the Stokes-Wilson equation [12]

$$\varepsilon = \frac{\beta}{4tan\theta} \quad (2)$$

The dislocation density of the synthesised Mg doped TiO_2 nanoparticles is 6.0122 x 10^{15} and the microstrain is 5.7352 x 10^{-3}.

3.2 UV-Visible Spectroscopy

The optical characteristics are examined by UV-visible spectroscopy. The absorption and band gap spectra are shown in figures 3(a) and 3(b). The strong absorption peak is observed at 279 nm in figure 3(a). The optical band gap was estimated using Tauc's plot. The $(\alpha h\nu)^2$ vs. hν plot was used to determine the optical band gap by extrapolating the linear portion of the curve to the hν axis [13]. The determined optical band gap is 2.77 eV, which is in good agreement with the reported value in the literature [14]. It indicates that the prepared nanomaterial is a semiconducting material.

S. No	2θ (deg)	FWHM (deg)	d- spacing (Å) [Exp]	d- spacing (Å) [Theo]	Crystalline size (nm)	δ x 10^{15} m^2	ε x 10-3
1	25.38	0.7872	3.5090	3.5077	10.3505	9.3342	15.2538
2	31.68	0.1574	2.8244	2.8226	52.4923	0.3629	2.4206
3	40.57	0.4723	2.2233	2.2224	17.9432	3.1059	5.5755
4	45.41	0.1968	1.9972	1.9961	43.7808	0.5217	2.0522
5	53.63	0.4723	1.7088	1.7076	18.8581	2.8119	4.0770
6	56.31	0.4723	1.6336	1.6326	19.0891	2.7442	3.8506
7	62.54	1.5744	1.4850	1.4842	5.9067	28.6622	11.3118
8	75.14	0.2362	1.2643	1.2634	42.4562	0.5547	1.3397

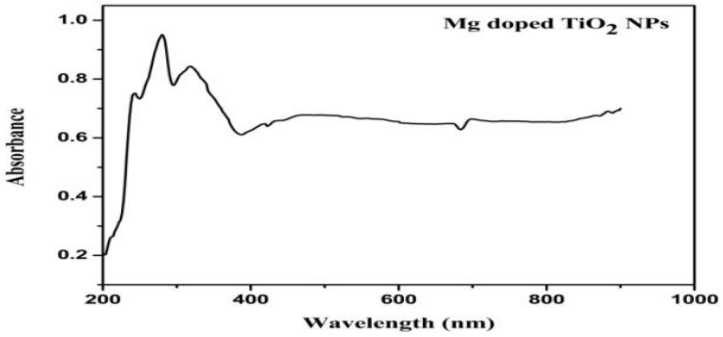

Figure 3(a) Absorbance spectra

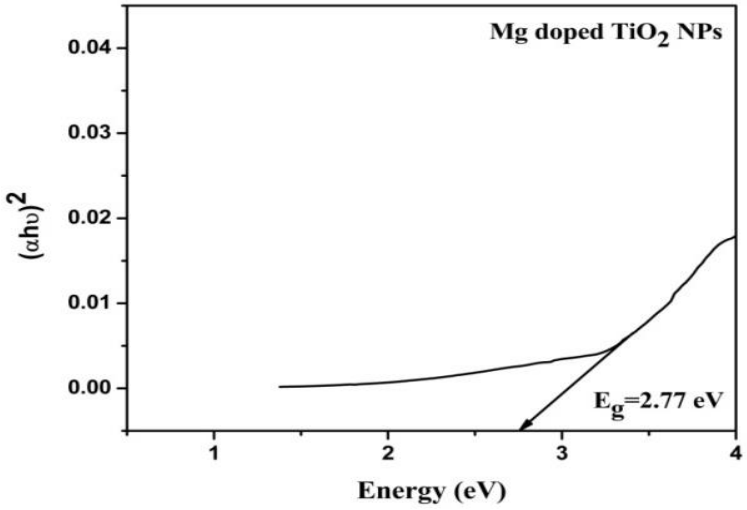

3(b) Band gap spectra of Mg doped TiO_2

3.3 Fourier Transform Infrared Spectroscopy

The FTIR spectrum in the range of 4000-400 cm^{-1} is shown in figure 4. The stretching vibration of the O-H bond is responsible for the peak at 3426 cm^{-1}. The peaks are around 2926 cm^{-1} to 1100 cm^{-1}, which corresponds to the pytochemicals like protein, crude fat, carbohydrate, fibre, saponins, tannins, flavanols, terpenoids, steroids and glycosides in the leaf extract. The peaks in the region of 1100-1000 cm-1 are due to the vibrational modes of the Ti-O-Mg bond [15]. The Ti-O-Ti bond is responsible for the absorption peak around 500 cm^{-1} [16]. The FTIR results confirm the presence of synthesised Mg-doped TiO_2 nanoparticles in the 1100-1000 cm^{-1} region.

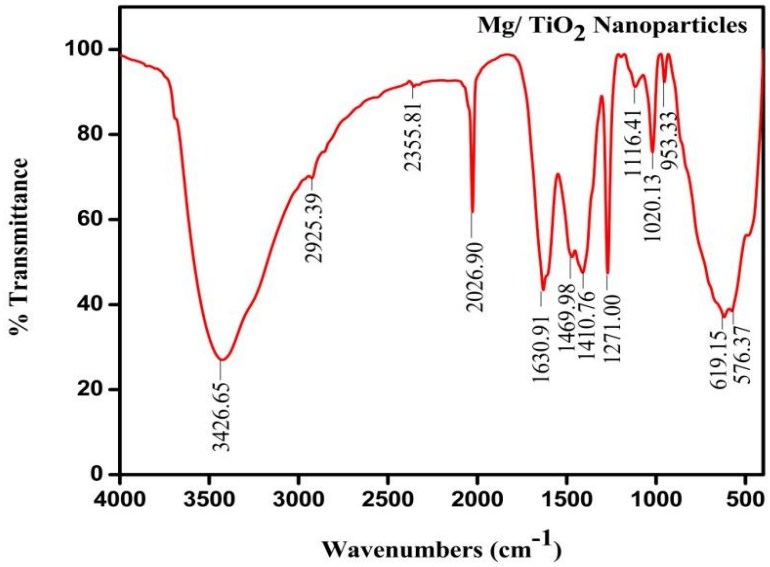

Figure 4. FTIR spectrum of Mg doped TiO_2 nanoparticles

3.4 Morphological and compositional analysis

SEM was used to analyse the surface morphology of the prepared sample. The SEM image of the prepared nanoparticles is shown in figure 5. It implies that the particles are spherical and elongated in shape and that they are agglomerated. The weight and atomic percentage of the synthesised Mg doped TiO_2 nanoparticles are determined using Energy Dispersive X-ray Spectroscopy. The EDX spectrum is displayed in figure 6. The Mg, Ti and O elements are present in the EDX spectrum, which confirms the formation of Mg doped TiO_2

nanoparticles. The atomic and weight percentages of the synthesised Mg doped TiO_2 nanoparticles are given in table 2.

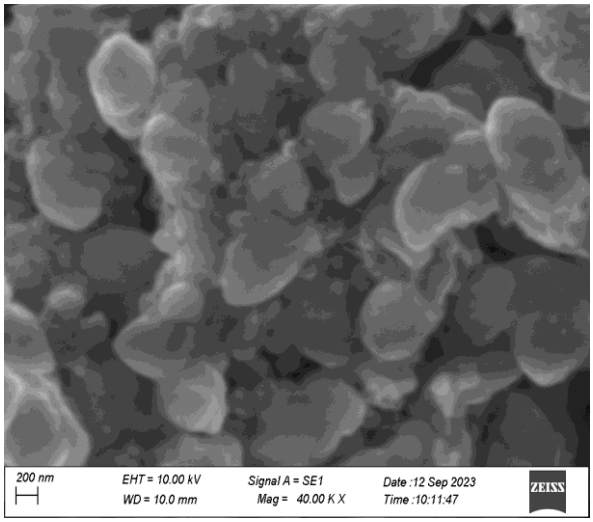

Figure 5. SEM images of Mg doped TiO_2 nanoparticles

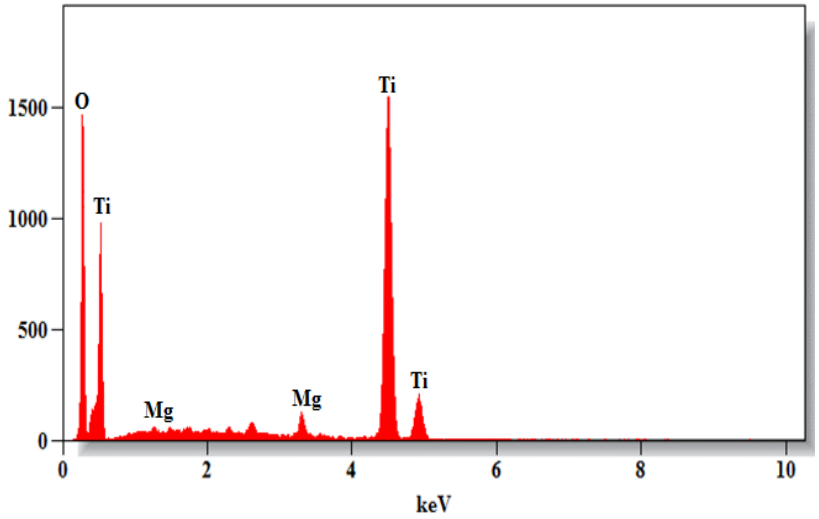

Figure 6. EDX spectrum of the synthesised Mg doped TiO_2 nanoparticles

Element	Weight %	Atomic %
Mg	12.23	15.66
Ti	41.99	30.19
O	45.78	54.15
Total	100.00	100.00

Table. 2. Elemental percentages of the prepared Mg doped TiO_2 Nanoparticles

3.5 Cyclic Voltammetry analysis

The electrochemical properties of the sample were investigated using cyclic voltammetry (CV). The experiments were carried out in a three-electrode configuration using modified magnesium doped titanium dioxide-glassy carbon as a working electrode, platinum wire as a counter electrode and calamol electrode as reference electrodes in a 0.1 M KOH salt bridge solution [17]. Figure 7 (a) shows the cyclic voltammetry of modified GCE with Mg doped TiO_2 nanoparticles at different scan rates between the potential -2.0 to +2.0. The plot between the scan rate and the specific capacitance of Mg doped TiO_2 NPs was depicted in figure 7 (b). The specific capacitance of Mg doped TiO_2 nanoparticles can be calculated by Eqn. 3 and listed in table 3 for various scan rates.

$$C_s = \frac{A}{mK\Delta V} \tag{3}$$

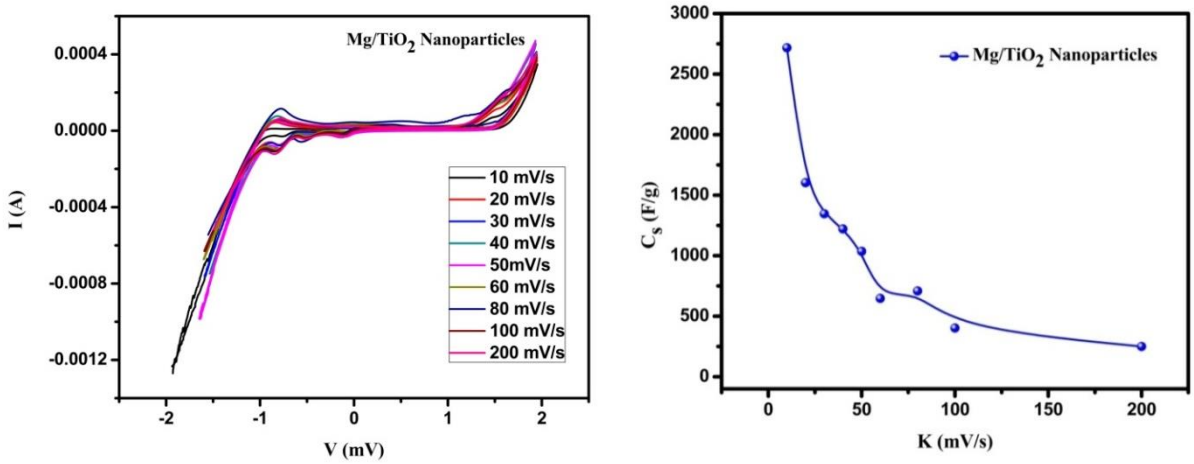

Figure 7. (a) CV for TiO_2 NPs (b) Cs vs K for TiO_2 NPs

Table 3. Scan rate and their specific capacitance for Mg doped TiO_2 nanoparticles

Scan rate (mV/s)	10	20	30	40	50	60	80	100	200
Specific Capacitance Cs (F/g)	2720	1600	1350	1220	1040	648	709	403	250

The reduction and oxidation peaks are discernible from the CV curves. This implies that the electrochemical capacitance of the Mg doped TiO_2 electrode is a result of pseudocapacitance. The current under the curve gradually increased with scan rate; we determined that the voltammetric current is directly proportional to scan rate, which is a good indicator of supercapacitive behavior. The specific capacitance values of the Mg doped TiO_2 electrode generally decreased as the scan rate increased. It is well known that at very low scan rates, the specific capacitance values are higher because the ions have more time to enter and occupy the electrode pores and build the electric double layers required to provide higher capacitance [18]. At slower scan rates, K+ from the electrolyte can be injected into practically all of the accessible pores on the surface as well as inside the Mg doped TiO_2 electrode. This leads to both a high capacitance and a high efficiency of Mg doped TiO_2 for the redox reaction. At higher scan rates, the K+ ions from the electrolyte do not have enough time to enter the interior portion of the Mg doped TiO_2 electrode material, making it impossible to access all available sites, resulting in surface adsorption. Due to their slow rate of movement in the electrolyte, the incomplete redox reaction results in decreased capacitance [19]. The prepared material exhibits a high specific capacitance of 2720 F/g at 10 mV/s scan rate. Thus, the cyclic voltammetry analysis reveals that Mg doped TiO_2 nanoparticles will be a promising electrode material for high-performance supercapacitors.

3.6 Electrochemical Impedance Spectroscopy

Electrochemical Impedance Spectroscopy (EIS) is an effective technique for analyzing the interfacial characteristics of electrodes with surface modifications and offers useful details on the impedance change at the electrode surface. EIS use the frequency sweep of a minuscule AC voltage modulated across DC bias to obtain the equivalent circuit. The circuit was generated by plotting the real and imaginary impedance parts (Nyquist diagram) [20]. The charge transfer resistance caused by the faradaic redox reaction forms a semicircle in the higher frequency zone and a straight line in the lower frequency region, proving the electrode's pseudocapacitive behavior. Semicircle size in the high frequency range denotes the dominant resistive nature of the supercapacitor system consisting of electrode/electrolyte/current collector. The Mg doped TiO_2 electrode Nyquist plot showed an extremely straight 45° line that was derived from the Warburg impedance and indicated a diffusion-limited electrochemical process, as well as a clearly defined semicircle on a high frequency area that was derived from the response of R_{ct} and C_{dl}. The R_{ct} of 681 Ω proved that significant diffusion and the redox reaction occurred on the electrode surface. The Mg doped TiO_2 nanoparticles that had been modified subsequent to it showed Warburg impedance at low frequencies and a tiny semicircle at higher frequencies [21-23]. Mg doped TiO_2 has a solution resistance (R_s) and pore resistance (R_p) of 47 Ω and 729 Ω respectively. The prepared sample has a double-layer capacitance of 1.63 nF. The Nyquist plot for Mg doped TiO_2 nanoparticles and a Randles-equivalent circuit is shown in Figures. 8(a) and 8(b).

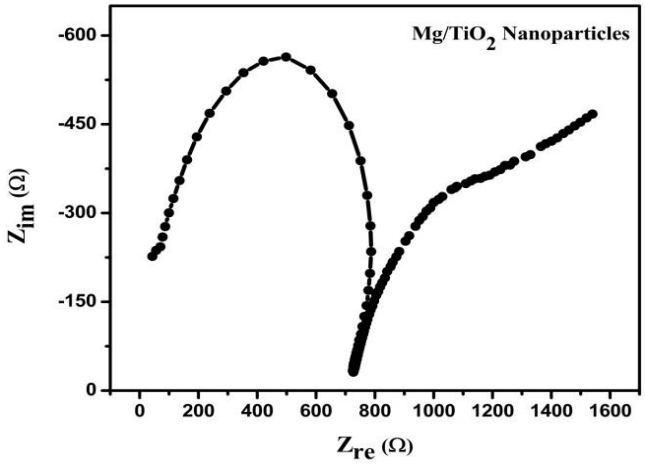

Figure 8. (a) Nyquist plot for Mg doped TiO_2 nanoparticles

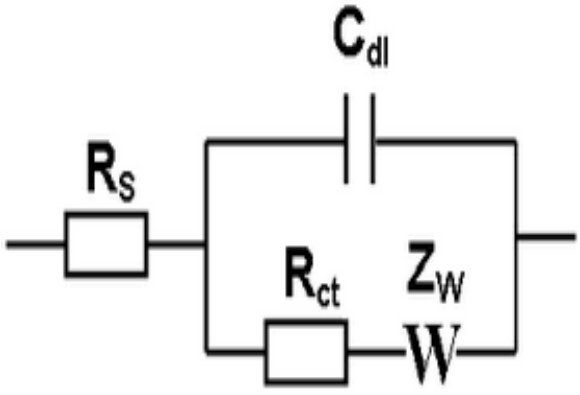

Figure 8. (b) Randles equivalent circuit

3.7 Photocatalytic activity

Artificial dyes are used in various industries, such as textiles, cosmetics, paper and plastics. Synthetic dyes are harmful to humans and can cause mutagenesis, carcinogenesis and a variety of skin problems. Photocatalytic dye degradation is more efficient than chemical or physical processes [24-25]. The most efficient application of Mg doped TiO_2 nanoparticles is dye degradation. The photocatalytic activity of prepared sample was analysed by Methylene blue (MB) and Congo red (CR) under visible light irradiation. The MB and CR for 10 and 20 mg concentrations at 650 nm and 498 nm absorbance were measured using a UV-vis spectrophotometer. Figure 9 depicts the graphical representation of MB and CR dye at 650 nm and 498 nm absorbance and the degradation of MB and CR dye at 10 and 20 mg concentrations is listed in table 4.

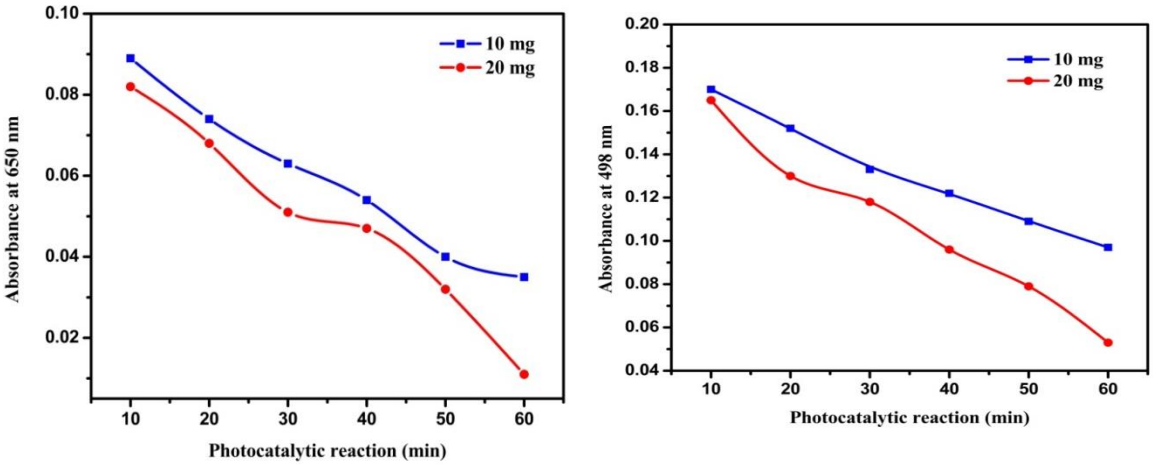

Figure 9. Visible light absorbance spectra of MB and CR dye

The photo-removal efficiency percentage of the synthesised was estimated from the equation (3)

$$\% \text{ Photo-removal efficiency} = C_0 - C \,/\, C_0 \times 100 \quad (3)$$

where C_0 is the initial concentration of dye and C is the concentration of dye after photo-irradiation [26].

Table 4. The degradation data of MB and CR dye

Mg doped TiO_2 nanoparticles as a catalyst				
Degradation Time	**Degradation of Methylene blue**		**Degradation of Congo red**	
Minutes	**10 mg**	**20 mg**	**10 mg**	**20 mg**
10	0.089	0.082	0.17	0.165
20	0.074	0.068	0.152	0.13
30	0.063	0.051	0.133	0.118
40	0.054	0.047	0.122	0.096
50	0.04	0.032	0.109	0.079
60	0.035	0.016	0.097	0.043

The degradation percentages of MB and CR at 10 and 20 mg are 61%, 80%, and 43%, 74% respectively. The photocatalytic activity of the Mg doped TiO_2 nanoparticles shows greater degrading efficiency of MB compared to CR.

4. Conclusion

The Mg doped TiO_2 nanoparticles were prepared using solanum torvum leaf extract by green synthesis method. The synthesised nanoparticles were characterized by XRD, UV, FTIR, EDX and photocatalytic activity. The XRD spectrum confirms the orthorhombic structure of TiO_2 nanoparticles. The average crystalline size is 26 nm. The determined optical band gap of is 2.77 eV. The presence of functional group was confirmed by FTIR spectrum and vibrational modes of the Ti-O-Mg bond were observed at 1100-1000 cm^{-1} region. The SEM images exhibit that the prepared material is spherical and oval in shape and also agglomerated. The purity of the Ti, O and Mg was confirmed by the EDX analysis. The cyclic voltammetry measurements indicated that these electrodes have a well-specific capacitance of 2720 F/g at 10 mV/s scan rate. The electric double-layer capacitance of the sample is calculated using impedance spectroscopy and it is found to be 1.6 nF. The electrochemical analysis reveals that Mg doped TiO_2 nanoparticles will be a promising electrode material for high-performance supercapacitors. The prepared nanoparticles exhibit significant photocatalytic degradation at 20 mg concentrations of Congo red (CR) and Methylene blue (MB). MB has greater degrading efficiency compared to CR.

References

[1] Albrecht, Matthew A., Cameron W. Evans, and Colin L. Raston. Green chemistry and the health implications of nanoparticles. Green chemistry 8(5) (2006): 417-432.

[2] Agnihotri, Mithila, Swanand Joshi, Ameeta Ravi Kumar, Smita Zinjarde, and Sulabha Kulkarni. Biosynthesis of gold nanoparticles by the tropical marine yeast Yarrowia lipolytica NCIM 3589. Materials Letters 63(15) (2009): 1231-1234.

[3] Rajakumar, G., A. Abdul Rahuman, B. Priyamvada, V. Gopiesh Khanna, D. Kishore Kumar, and P. J. Sujin. Eclipta prostrata leaf aqueous extract mediated synthesis of titanium dioxide nanoparticles. Materials Letters 68 (2012): 115-117.

[4] Dobrucka, Renata. The biological synthesis of anatase titanium dioxide nanoparticles using Arnicae anthodium extract. Bulg. Chem. Commun 49(3) (2017): 595-599.

[5] Patidar, Vivek, and Preeti Jain. Green synthesis of TiO_2 nanoparticle using Moringa oleifera leaf extract. Int Res J Eng Technol 4(3) (2017): 1-4.

[6] Nithya, N., S. Gopi, and G. Bhoopathi. An Amalgam of Mg-Doped TiO_2 Nanoparticles Prepared by Sol–Gel Method for Effective Antimicrobial and Photocatalytic Activity. Journal of Inorganic and Organometallic Polymers and Materials 31 (2021): 4594-4607.

[7] Kirthi, A. Vishnu, A. Abdul Rahuman, G. Rajakumar, S. Marimuthu, T. Santhoshkumar, C. Jayaseelan, G. Elango, A. Abduz Zahir, C. Kamaraj, and A. Bagavan. Biosynthesis of titanium dioxide nanoparticles using bacterium Bacillus subtilis. Materials Letters 65, no. 17-18 (2011): 2745-2747.

[8] Zahra, Samreen, Sania Mazhar, Sarwat Zahra, Hira Idrees, and Ali Hussnain. Synthesis and characterization of magnesium doped titania for photocatalytic degradation of methyl red. Matéria (Rio de Janeiro) 27 (2022): e13160.

[9] Athira, K., K. T. Merin, T. Raguram, and K. S. Rajni. Synthesis and characterization of Mg doped TiO_2 nanoparticles for photocatalytic applications. Materials Today: Proceedings 33 (2020): 2321-2327.

[10] Dubey, Krishna Chandra, Anam Zaidi, and Ram Raseele Awasthi. Environmentally benign structural, topographic, and sensing properties of pure and Al-doped ZnO thin films. ACS omega 7, no. 33 (2022): 28946-28954.

[11] Shaik, Khajamuswareen, and Sandhya Cole. "Comparative Study of Crystallite Size from XRD and TEM Results for Pure and V_2O_5 Doped CdO-$FePO_4$ Composite Nanopowders." Physical Chemistry Research 11, no. 2 (2023): 241-251.

[12] Stokes, A. R., and A. J. C. Wilson. The diffraction of X rays by distorted crystal aggregates-I. Proceedings of the physical society 56(3) (1944): 174.

[13] Senthilkumar, Subramanian, Mahalingam Ashok, Lellala Kashinath, Chinnappanadar Sanjeeviraja, and Annamalai Rajendran. Phytosynthesis and characterization of TiO_2 nanoparticles using Diospyros ebenum leaf extract and their antibacterial and photocatalytic degradation of crystal violet. Smart Science 6(1) (2018): 1-9.

[14] Shakir, Sehar, Hafiz M. Abd-ur-Rehman, Kamran Yunus, Mitsumasa Iwamoto, and Vengadesh Periasamy. Fabrication of un-doped and magnesium doped TiO_2 films by aerosol assisted chemical vapor deposition for dye sensitized solar cells. Journal of Alloys and Compounds 737 (2018): 740-747.

[15] Ramimoghadam, Donya, Samira Bagheri, and Sharifah Bee Abd Hamid. Biotemplated synthesis of anatase titanium dioxide nanoparticles via lignocellulosic waste material. BioMed research international 2014 (2014).

[16] Manojkumar, M. S., S. Venkatesan, and S. Pandiarajan. Morphological, optical and structural properties of pure, zinc and magnesium doped TiO_2 nanoparticles for solar cell devices. Journal of Ovonic Research 18(1) (2022).

[17] J. Sackey, A. Nwanya, A. K. Bashir, N. Matinise, J. B. Ngilirabanga, A. E. Ameh, E. Coetsee, M. Maaza, Electrochemical properties of Euphorbia pulcherrima mediated copper oxide nanoparticles, Materials Chemistry and Physics. 244 (2020) 122714.

[18] S. M. Jogade, D. S. Sutrave, S. D. Gothe, Electrochemical analysis of cobalt oxide thin film for supercapacitor, International Journal of Advanced Research in Physical Science (IJARPS). 2(10) (2015) 36-41.

[19] F. Zhang, X. G. Zhang, L. Hao, Solution synthesis and electrochemical capacitance performance of Mn_3O_4 polyhedral nanocrystals via thermolysis of a hydrogen-bonded polymer, Materials Chemistry and Physics. 126(3) (2011) 853-858.

[20] M. M .Vinay, Y. A. Nayaka, Iron oxide (Fe_2O_3) nanoparticles modified carbon paste electrode as an advanced material for electrochemical investigation of paracetamol and dopamine, Journal of Science: Advanced Materials and Devices, 4(3) (2019) 442-50.

[21] B. Y. Chang, S. M. Park, Electrochemical impedance spectroscopy, Annual review of analytical chemistry. 3 (2010) 207–229.

[22] M. Manickam, V. Ponnuswamy, C. Sankar, R. Suresh, R. Mariappan, A. Chandra Bose, J. Chandrasekaran, Structural, optical, electrical and electrochemical properties of Fe: Co_3O_4 thin films for supercapacitor applications, Journal of Materials Science: Materials in Electronics. 28 (2017) 18951-65.

[23] Donghai Lin, Thompson Tank, D. Jed Harrison, W. E. Lee, A. B. Jemere, A regenerating ultrasensitive electrochemical impedance immunosensor for the detect ion of adenovirus, Biosensors and Bioelectronics. 68 (2015) 129–134.

[24] Sankar, Renu, Perumal Manikandan, Viswanathan Malarvizhi, Tajudeennasrin Fathima, Kanchi Subramanian Shivashangari, and Vilwanathan Ravikumar. Green synthesis of colloidal copper oxide nanoparticles using Carica papaya and its application in photocatalytic dye degradation. Spectrochimica Acta Part A: Molecular and Biomolecular Spectroscopy 121 (2014): 746-750.

[25] Ganesan, S., I. Ganesh Babu, D. Mahendran, P. Indra Arulselvi, N. Elangovan, N. Geetha, and P. Venkatachalam. Green engineering of titanium dioxide nanoparticles using Ageratina altissima

(L.) King & HE Robines. medicinal plant aqueous leaf extracts for enhanced photocatalytic activity. Ann. Phytomed 5(2) (2016): 69-75.

[26] Abhilash, M. R., G. Akshatha, and S. Srikantaswamy. Photocatalytic dye degradation and biological activities of the Fe_2O_3/Cu_2O nanocomposite. RSC Adv 9: 8557–8568. (2019).